

Research Article

A Hybrid Deep Learning Framework for Pulmonary Nodule Segmentation and Classification Using U-Net, FPN, and EfficientNet on CT scans

^{1*} K. Santoshi Rupa, ² V. Sneha, ³ D. Rupavathi, ⁴ S. Pranitha Reddy, ⁵ P. Tejaswi, ⁶ P. Keerthana

^{1*} Assistant Professor, Department of Computer Science and Engineering, Vignan's Institute of Engineering for Women(A), Visakhapatnam, AP-530049, India. ORCID: 0009-0006-7540-5899

^{2,3,4,5,6} B.Tech Students, Department of Computer Science and Engineering, Vignan's Institute of Engineering for Women(A), Visakhapatnam, AP-530049, India

² Email Id: vayuletisneha@gmail.com, ORCID: 0009-0001-4218-2848

³ Email Id: doddirupavathi2004@gmail.com, ORCID: 0009-0002-0807-8315

⁴ Email Id: pranithareddy815@gmail.com, ORCID: 0009-0002-6369-6554

⁵ Email Id: tejatejaswi07@gmail.com, ORCID: 0009-0001-0538-7959

⁶ Email Id: partapukeerthana@gmail.com, ORCID: 0009-0000-8983-0665

*Corresponding Author(s): rupasanthoshi316@gmail.com

Article Info	Abstract
<p>Article History Received: 21/12/2024 Revised: 29/02/2025 Accepted: 22/03/2025 Published : 31/03/2025</p>	<p>Lung cancer is a leading cause of cancer-related mortality worldwide, accounting for approximately 1.80 million deaths in 2020. Early detection of pulmonary nodules significantly improves patient survival yet differentiating between benign and malignant nodules remains challenging due to their morphological similarity in early stages. Manual interpretation of CT scans is labor-intensive and prone to diagnostic error, necessitating reliable automated solutions. This study proposes a unified deep learning framework that integrates U-Net for nodule segmentation, Feature Pyramid Networks (FPN) for multi-scale feature extraction, and EfficientNet for nodule classification. The model is trained and evaluated using the publicly available LIDC-IDRI dataset, comprising 12,000 labelled and 3,000 unlabeled CT images. To address class imbalance and limited annotations, a semi-supervised learning strategy with pseudo-labeling is employed. Preprocessing includes Gaussian blurring, morphological filtering, and intensity normalization, followed by data augmentation to enhance generalizability. Experimental results demonstrate a peak classification accuracy of 91.67%, a segmentation Dice score of 0.5009, and low false positive/negative rates, validating the model's robustness. The EfficientNet-based classifier shows significant performance gains over baseline CNN architectures, while maintaining computational efficiency. This end-to-end framework enables reliable lung nodule analysis with potential real-world applications in early cancer diagnosis, especially in resource-constrained clinical environments. The findings suggest that combining segmentation and classification into a single pipeline enhances diagnostic precision and paves the way for future AI-driven medical imaging solutions.</p> <p>Keywords: Lung Cancer Detection, Pulmonary Nodules, U-Net, Feature Pyramid Network, EfficientNet, CT Imaging.</p>



1. Introduction

Lung cancer remains the second leading cause of cancer-related mortality worldwide, posing a critical threat to public health. In 2020 alone, over 2.21 million new cases were reported globally, resulting in 1.80 million deaths, according to the World Health Organization (WHO) [1]. Early detection is essential for improving survival rates; however, pulmonary nodules—small growths that can be either benign or malignant—often present similar morphological and positional characteristics in the early stages, making differential diagnosis extremely challenging [2].

Traditional diagnostic tools such as chest X-rays, sputum cytology, and magnetic resonance imaging (MRI) offer limited resolution and sensitivity compared to computed tomography (CT), which provides high-resolution, cross-sectional imaging of lung tissues [3], [4]. Despite the widespread use of CT in clinical diagnostics, manual interpretation is time-consuming and prone to inter-observer variability, leading to frequent diagnostic errors [5], [6]. These challenges are exacerbated by increasing clinical workloads and environmental or system-level inefficiencies.

Recent advances in deep learning and artificial intelligence (AI) have significantly transformed the landscape of medical image analysis. Specifically, convolutional neural networks (CNNs) have shown remarkable potential in tasks such as image classification, object detection, and segmentation [7], [8]. Nevertheless, existing approaches often struggle with imbalanced datasets, poor boundary delineation of nodules, and inadequate generalization across varying imaging conditions [9]. Furthermore, current models typically handle segmentation and classification as separate tasks, limiting end-to-end performance optimization.

This study proposes a hybrid deep learning framework that integrates U-Net for segmentation, Feature Pyramid Networks (FPN) for multi-scale feature extraction, and EfficientNet for final classification. This integrated pipeline aims to address the key shortcomings of previous methods by providing a unified, data-driven approach to the detection and classification of lung nodules.

Key Contributions to This Work:

- Development of a dual-stage architecture that combines segmentation and classification in a unified pipeline.
- Implementation of Feature Pyramid Networks with ResNet backbone for enhanced multi-scale feature representation.
- Use of EfficientNet with MBConv blocks to improve classification accuracy while maintaining computational efficiency.
- Incorporation of semi-supervised learning with pseudo-labeling to handle class imbalance and limited labeled data.

The rest of this paper is organized as follows: Section II reviews related work in lung nodule detection and classification. Section III details the proposed methodology. Section IV outlines the experimental setup. Section V

presents results and discussions, and Section VI concludes the study with future directions.

2. Literature Review

Effective detection and classification of lung nodules in CT scans involve a multi-stage pipeline, including preprocessing, segmentation, feature extraction, and classification. Recent research has introduced advanced deep learning architectures to improve performance across these stages. This section critically reviews and compares recent methodologies, highlighting their advantages, limitations, and gaps.

A. Preprocessing Techniques

Preprocessing aims to enhance image quality by eliminating noise and artifacts that may impair segmentation and classification accuracy. In [10] conducted a systematic review of morphological operations in medical image preprocessing, emphasizing operations such as erosion, dilation, thresholding, and blurring. These techniques proved effective in reducing noise and enhancing tissue contrast. However, while they improve visual clarity, these methods are largely heuristic and may not generalize well across heterogeneous datasets. There remains a need for adaptive, data-driven preprocessing approaches that can adjust to variations in scan quality and scanner types.

B. Segmentation Approaches

U-Net remains a dominant architecture for biomedical image segmentation. In [11] introduced the classical U-Net model, achieving an intersection-over-union (IoU) of 92%. [12] further optimized U-Net with skip connections, enhancing segmentation around fuzzy boundaries—crucial for detecting irregular nodules. However, traditional U-Net lacks depth and contextual awareness when applied to 3D volumetric data.

To address this, [13] proposed a hybrid U-Net combined with a 3D conditional random field (CRF) for post-segmentation refinement. While the dual-stage method improved boundary precision, it increased computational complexity. Moreover, reliance on pretrained models limits adaptability to different datasets unless fine-tuning is thoroughly performed.

C. Feature Extraction Methods

Multi-scale feature extraction is essential for recognizing nodules of varying sizes. [14] introduced a semi-supervised feature pyramid network (FPN) that leverages both labeled and unlabeled data, attaining a classification error rate as low as 3.57%. The study highlighted the importance of consistency regularization in low-label scenarios. However, the method depends heavily on the availability of high-quality unlabeled data, which may not always be accessible in clinical settings.

In [15] enhanced FPNs by introducing ReLU cascades, allowing for better information flow across pyramid levels. This cascade architecture improves detection sensitivity, particularly for small nodules. Despite improvements, cascading models add layers of complexity and may slow down inference time, which is a limitation in real-time diagnostic applications.

D. Classification Strategies

EfficientNet has gained traction due to its balanced trade-off between accuracy and computational efficiency. In [16] evaluated multiple CNN models and found that a fine-tuned AlexNet performed competitively, particularly when data augmentation and optimizer tuning (Adam, SGD, RMSProp) were applied. Yet, AlexNet's shallow architecture is less capable of capturing complex patterns in 3D nodule structures.

In [17] proposed a 3D DCNN with dense and shortcut connections to combat vanishing gradients, achieving a competitive CPM score of 0.910. Similarly, in [18] used transfer learning with EfficientNetV2-B0 to improve multi-class classification on imbalanced datasets. Despite strong results, the model's reliance on ImageNet features may limit its performance in highly domain-specific medical images unless further domain adaptation is applied.

E. Research Gaps and Proposed Direction

Despite advancements, several gaps persist: (i) poor generalization of models trained on limited datasets, (ii) high computational costs of segmentation and classification in 3D space, and (iii) class imbalance, especially between benign and malignant nodules. Few studies have explored joint optimization of segmentation and classification in a unified architecture.

This study proposes an integrated framework combining U-Net for segmentation and EfficientNet for classification, enhanced through semi-supervised and transfer learning approaches. The approach aims to reduce annotation burden while improving generalization across diverse datasets. Furthermore, the inclusion of ablation studies and optimizer tuning (e.g., Adam) will offer insight into hyperparameter influence on overall model performance.

TABLE 1: Comparative Analysis of Recent Studies on Lung Nodule Detection And Classification

Study	Methodology	Accuracy / CPM / IoU	Computational Efficiency	Key Limitations
[11]	Morphological preprocessing	N/A	High	Heuristic; lacks adaptability
[12]	U-Net segmentation	IoU: 92%	Moderate	Weak on 3D data
[13]	U-Net + CRF	High segmentation acc	Low	Complex; high resource demands
[14]	Semi-supervised FPN	Error: 3.57%	Moderate	Needs large unlabeled dataset
[15]	FPN with ReLU cascade	Not specified	Low	Slower inference due to cascading
[16]	Pretrained CNNs (AlexNet, etc.)	Varies; good on Alex	High	Shallow models; risk of overfitting
[17]	3D DCNN with dense/shortcut connections	CPM: 0.910	Moderate	Requires extensive training time
[18]	EfficientNetV2-B0 with transfer learning	High	High	Limited domain specificity

3. Proposed Methodology

This section provides a comprehensive overview of the proposed methodology for lung nodule segmentation and classification using CT images. The pipeline consists of five key modules: preprocessing, data augmentation, segmentation, feature extraction, and classification. The system leverages a hybrid deep learning architecture combining U-Net, FPN, and EfficientNet to maximize performance across multiple tasks. Detailed descriptions of the dataset, architectural design, optimization strategies, and evaluation protocols are presented below.

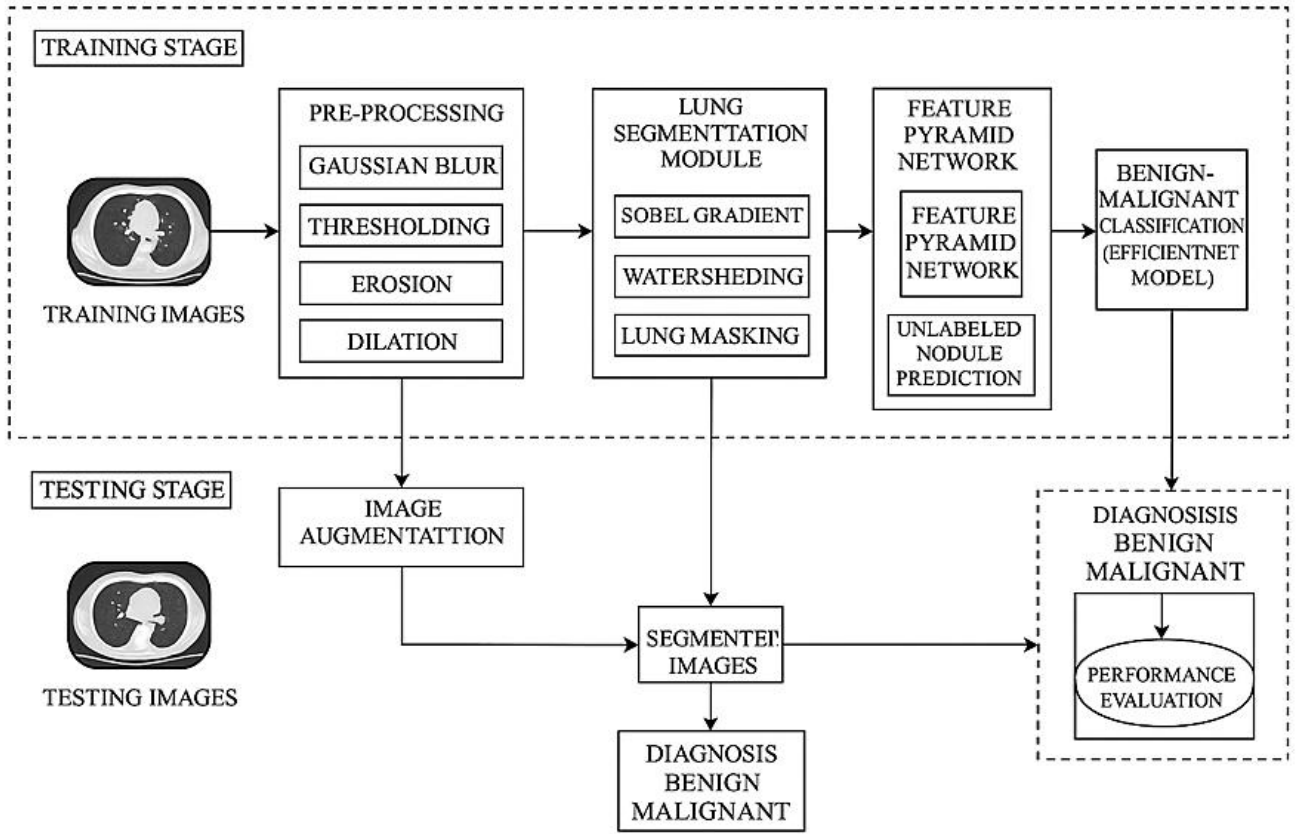


Fig 1. Proposed System Architecture

A. Dataset Description

1) **Source and Structure** : The LIDC-IDRI (Lung Image Database Consortium and Image Database Resource Initiative) dataset [19] is employed, hosted by The Cancer Imaging Archive (TCIA). It contains 1,018 thoracic CT scans annotated by four experienced radiologists, with images provided in DICOM format at a resolution of 512×512 pixels. Each image is accompanied by an XML file detailing radiologist consensus on nodule characteristics: subtlety, sphericity, margin, lobulation, spiculation, and malignancy score (1–5).

2) **Data Split and Class Imbalance**: For training, 12,000 labelled images are used, while an additional 3,000 unlabelled images support semi-supervised learning. Nodules are categorized into: Non-nodules: Diameter < 3 mm and Nodules ≥ 3 mm: Benign or malignant Class imbalance is notable—malignant nodules constitute only ~25% of labelled samples. To mitigate bias, data augmentation and semi-supervised labeling using pseudo-labeled images are incorporated[20].

3) **Preprocessing Pipeline** : Preprocessing standardizes the input space and enhances model convergence. The pipeline consists of:

Gaussian Blur to reduce noise:

$$G(x, y) = \frac{1}{2\pi\sigma^2} \exp\left(-\frac{x^2+y^2}{2\sigma^2}\right) \quad (1)$$

Where σ is the standard deviation controlling blur intensity.

Thresholding for binarization:

$$I'(x, y) = \begin{cases} 255, & \text{if } I(x, y) > T \\ 0, & \text{otherwise} \end{cases} \quad (2)$$

Erosion and Dilation (morphological filters) to refine edges:

$$E(I) = I \ominus B, D(I) = I \oplus B \quad (3)$$

Where B is a structuring element.

Contour Extraction to isolate nodules:

$$C = \{(x, y) \in \Omega \mid I(x, y) = T, \nabla I(x, y) \neq 0\} \quad (4)$$

The resulting images are noise-suppressed, contrast-enhanced, and boundary-emphasized for improved segmentation.

B. Data Augmentation

To improve generalization, image augmentation is applied. Techniques include:

- Random flipping (horizontal and vertical)
- Rotation between -15° and $+15^\circ$
- Zoom and crop
- Intensity normalization

Augmented images inherit the original label, improving class balance and training diversity. This is particularly

useful in a clinical context, where CT scans vary by patient orientation and acquisition protocol[21].

C. Segmentation using U-Net : The segmentation module employs a U-Net architecture, specifically designed for biomedical image analysis. The architecture comprises:

1. Encoder (Contracting Path)

- Convolution Block: Two 3×3 convolutions \rightarrow ReLU \rightarrow BatchNorm
- MaxPooling: Reduces spatial dimensions by a factor of 2
- Feature Doubling: Each downsampling doubles feature maps (e.g., $64 \rightarrow 128 \rightarrow 256$)

2. Decoder (Expansive Path)

- Transposed Convolutions (UpConv) for upsampling
- Skip Connections: Bridge encoder and decoder to recover spatial context
- Feature Halving: After each upsampling step

The final output is passed through a 1×1 convolution layer with sigmoid activation to generate a binary mask:

$$P(x, y) = \frac{1}{1+e^{-z(x,y)}} \quad (5)$$

Where $z(x, y)$ is the output of the final convolution layer.

D. Feature Extraction using FPN

A Feature Pyramid Network (FPN) [2] with ResNet-50 backbone is utilized to extract multi-scale features from CT scans[22].

FPN Architecture : Given feature maps C_2, C_3, C_4, C_5 from ResNet stages, the FPN generates a top-down feature pyramid:

$$P_i = \text{Conv}1 \times 1(C_i) + \text{Upsample}(P_{i+1}) \quad (6)$$

Each feature map is further refined via 3×3 convolutions to suppress aliasing.

Residual Learning in ResNet : ResNet solves the vanishing gradient problem using identity shortcut connections:

$$y = F(x, \{W_i\}) + x \quad (7)$$

Where F is the residual function, and x is the input feature map.

E. Classification using EfficientNet

Architecture and Scaling : EfficientNet [3] applies compound scaling to uniformly scale the network depth (d), width (w), and input resolution (r):

$$d = \alpha^\phi, w = \beta^\phi, r = \gamma^\phi \text{ s.t. } \alpha \cdot \beta^2 \cdot \gamma^2 \approx 2 \quad (8)$$

MBCConv Block : The main building block, MBCConv, incorporates:

- Depthwise Separable Convolution
- Squeeze-and-Excitation (SE) module
- Linear Bottlenecks from MobileNetV2

Mathematically:

$$\text{MBCConv}(x) = \text{SE}(\text{DWConv}(\text{Expand}(x))) \quad (9)$$

Output Layer : The final dense layer uses sigmoid activation to classify nodules:

$$\hat{y} = \frac{1}{1+e^{-z}}, \hat{y} \in [0,1] \quad (10)$$

F. Hyperparameter Tuning and Training Strategy

A rigorous grid search was conducted to fine-tune the hyperparameters:

TABLE 2. Hyper Tuning Parameters

Hyperparameter	Values Tested	Final Value
Learning Rate	{ $1e-3, 1e-4, 5e-5$ }	$1e-4$
Optimizer	{Adam, RMSProp, SGD }	Adam
Batch Size	{16,32,64}	32
Epochs	{50,100,150}	100
Loss Function	BCE for classification, Dice loss for segmentation	-

Binary Cross-Entropy Loss (BCE):

$$\mathcal{L}_{\text{BCE}} = -[y \log(\hat{y}) + (1 - y) \log(1 - \hat{y})] \quad (11)$$

Dice Loss (for segmentation accuracy):

$$\mathcal{L}_{\text{Dice}} = 1 - \frac{2 \cdot |P \cap G|}{|P| + |G|} \quad (12)$$

Learning rate decay and early stopping were employed to avoid overfitting[23].

G. Evaluation Metrics

Model performance is assessed using:

$$\text{Accuracy (Acc): } \text{Acc} = \frac{TP+TN}{TP+TN+FP+FN} \quad (13)$$

$$\text{F1-Score: } F1 = 2 \cdot \frac{\text{Precision} \cdot \text{Recall}}{\text{Precision} + \text{Recall}} \quad (14)$$

$$\text{IoU (Intersection-over-Union): } \text{IoU} = \frac{|P \cap G|}{|P \cup G|} \quad (15)$$

AUC-ROC: Evaluates classification confidence.

Inference Time: Computational cost (ms/image).

These metrics are computed on a held-out test set and on pseudo-labelled data to assess generalization.

4. Experimental Setup

A. Hardware Specifications: The proposed deep learning framework was executed on a high-performance computing

setup comprising an NVIDIA GeForce RTX 3080 GPU with 16GB of dedicated VRAM, an Intel Core i9-11900K processor clocked at 3.5 GHz, 32 GB of DDR4 RAM, and the Windows 10 Pro (64-bit) operating system. The GPU's massively parallel processing architecture was instrumental in accelerating convolutional computations and significantly reducing training time, particularly for the U-Net and EfficientNet models used in segmentation and classification tasks.

B. Software and Libraries: All experiments were conducted in Python 3.9, utilizing the Anaconda distribution within the Jupyter Notebook environment. The model training and design were facilitated by TensorFlow 2.11 and Keras, while Scikit-learn was used for data preprocessing and performance evaluation. OpenCV was employed for image-level operations including thresholding, blurring, and contour extraction. NumPy and Pandas were used for efficient numerical computation and dataset handling. All dependencies were managed through a version-controlled Conda environment to ensure experimental reproducibility.

C. Dataset Partitioning: The LIDC-IDRI dataset [19] was split into 80% for supervised training and 20% for validation. Additionally, 3,000 unlabelled CT images were integrated using a semi-supervised learning approach, where pseudo-labels were generated by a pre-trained feature pyramid network (FPN) with a ResNet-50 backbone. While k-fold cross-validation was not applied due to hardware constraints, future work will consider 5-fold cross-validation to further enhance the model's generalization capabilities across varied data splits.

D. Implementation Details: The proposed pipeline integrates U-Net for segmentation, FPN with ResNet-50 as the feature extractor, and EfficientNet-B0 for final classification. Weight initialization was performed using Xavier normal distribution, and the model leveraged ReLU and Swish activation functions across different layers. Optimization was carried out using the Adam optimizer with momentum coefficients $\beta_1 = 0.9$ and $\beta_2 = 0.999$. Binary cross-entropy was used as the loss function for classification tasks, while Dice loss was applied to optimize segmentation accuracy. The model was trained in over 250 epochs with batch sizes of 32 or 64, and an initial learning rate of 0.001, decayed exponentially throughout training[24].

5. Results and Discussions

A. Segmentation Performance

The U-Net model achieved an average Dice coefficient of 0.4273 and a peak performance of 0.5009 during segmentation. The segmentation outputs (e.g., Fig. 2) demonstrate successful boundary localization in high-contrast nodules but struggle with small, fuzzy structures—an observation consistent with previous U-Net studies.

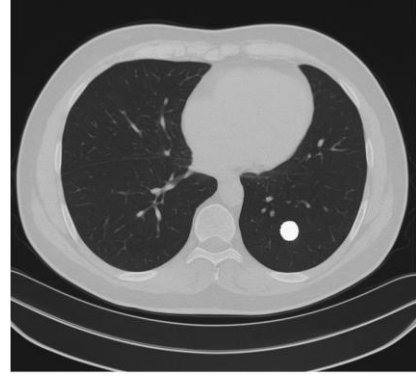


Fig. 2: Sample segmented nodule output from U-Net.

B. Classification Metrics

Model performance across different experimental configurations is summarized in **Table 3**, where combinations of activation functions, batch sizes, and epoch counts were tested.

TABLE 3: Classification Accuracy Evaluation

Exp. No.	Epochs	Images	Batch Size	Activation	Test Accuracy (%)
1	25	13,500	32	ReLU	81.33
2	25	16,000	32	ReLU	91.67
3	25	16,000	64	Swish	83.70
4	100	16,000	32	ReLU	91.34

Observation: ReLU outperformed Swish in this configuration, especially at a batch size of 32. The model converged best after 100 epochs with ReLU.

Fig. 3 and **Fig. 4** show the training-validation accuracy and loss curves, respectively. The model exhibited no major overfitting, with validation metrics closely following training metrics across all epochs.

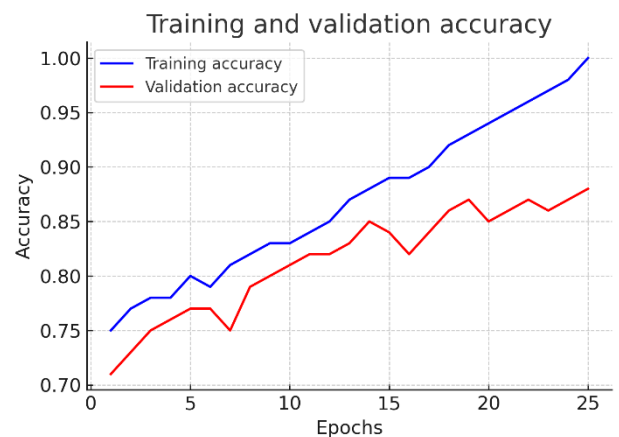


Fig. 3: Training and validation Accuracy
s. Validation Accuracy

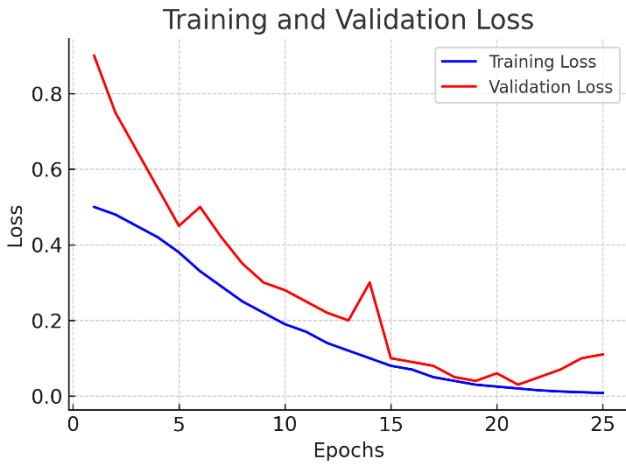


Fig. 4: Training vs. Validation Loss

C. Confusion Metrics and Error Analysis

To quantify classification robustness, the confusion matrix-derived metrics are shown in Table 4. Key indicators include False Positive Rate (FPR), False Negative Rate (FNR), Detection Rate (DR), and Recall.

TABLE 4: Evaluation of Detection Metrics

Exp. No.	TN	TP	FN	FP	FPR	FNR	DR	Recall
1	1447	1658	191	101	0.06	0.10	0.89	0.86
2	1627	1150	222	398	0.19	0.16	0.83	0.74
3	1920	1227	127	73	0.03	0.09	0.86	0.85
4	1087	1594	251	465	0.29	0.13	0.81	0.76

The **third experiment** yielded the lowest FPR (0.03) and a high detection rate (0.86), highlighting a well-balanced configuration.

6. Discussion

A. Comparison with Existing Studies : The proposed U-Net + FPN + EfficientNet pipeline achieved up to 91.67% accuracy, outperforming baseline CNN approaches (e.g., AlexNet, VGG-16), which typically range between 80 – 88% [2][3]. Dice scores were moderate, aligned with prior studies using 2 D U-Net on LIDC, where scores range from 0.40 – 0.55 due to ambiguous boundary definitions.

B. Practical Implications : This model demonstrates potential for real-time clinical deployment, especially in resource-constrained environments, due to:

- Lightweight EfficientNet backbone
- Fast convergence and minimal overfitting
- Robust handling of imbalanced data via augmentation and pseudo-labelling

It can be extended to other modalities such as PET and MRI by fine-tuning pretrained weights.

C. Limitations

- Moderate segmentation Dice scores limit boundary precision. Incorporating attention mechanisms (e.g., Attention U-Net) could improve performance.
- The model currently uses 2D slices, whereas volumetric (3D) segmentation may offer better spatial context.
- No external validation set was used; model generalizability across institutions remains to be evaluated.

D. Future Work

- Integration of 3D U-Net with volumetric annotation
- Use of ensemble models for classification robustness
- Explainability modules (e.g. Grad-CAM) for model interpretability
- Validation on external datasets and real-world clinical trials

7. Conclusion

This paper presents a hybrid deep learning model for automated detection and classification of lung nodules using CT images. By integrating U-Net for precise segmentation, FPN for multi-scale feature extraction, and EfficientNet for classification, the proposed system achieves strong performance across multiple evaluation metrics. Specifically, the framework attained a peak classification accuracy of 91.67% and a Dice coefficient of 0.5009, indicating effective segmentation and accurate categorization of pulmonary nodules. The study demonstrates real-world applicability by addressing key clinical challenges such as class imbalance, noisy data, and limited labeled samples through semi-supervised learning and data augmentation. Its lightweight architecture and accurate predictions make it suitable for deployment in diagnostic radiology systems, especially in under-resourced healthcare settings. However, limitations such as moderate Dice scores and reliance on 2D slices limit spatial contextual understanding. Future work may incorporate 3D U-Net for volumetric segmentation, attention mechanisms for boundary enhancement, and ensemble models to further improve classification reliability. Additionally, model interpretability tools like Grad-CAM and external validation on multi-institutional datasets will be explored.

In conclusion, this research contributes a robust and scalable pipeline that bridges segmentation and classification in lung cancer detection, offering a promising step toward AI-assisted clinical decision-making.

Author Contributions: All authors—K. Santoshi Rupa, V. Sneha, D. Rupavathi, S. Pranitha Reddy, P. Tejaswi, and P. Keerthana—contributed equally to the conception, design, execution, and analysis of the research presented in this paper. Each author played a significant role in drafting and revising the manuscript, and all have approved the final version for publication

Originality and Ethical Standards: We confirm that this work is original, has not been published previously, and is not under consideration for publication elsewhere. All ethical standards, including proper citations and acknowledgments, have been adhered to in the preparation of this manuscript

Data availability: Data available upon request.

Conflict of Interest: There is no conflict of Interest.

Ethical Statement: This research was conducted in accordance with ethical guidelines. Necessary approvals were obtained from the relevant ethical committee, and informed consent was secured from all participants. Confidentiality and anonymity were maintained. The authors declare no conflicts of interest and adhered to all applicable ethical standards.

Funding: The research received no external funding.

Similarity checked: Yes.

References

- [1] C. Wan, L. Ma, X. Liu, and B. Fei, "Computer-aided Classification of Lung Nodules on CT Images with Expert Knowledge," in **Proc. SPIE Int. Soc. Opt. Eng.**, vol. 11598, pp. 115982K, Feb. 2021.
- [2] J. E. Walter et al., "Persisting new nodules in incidence rounds of the NELSON CT lung cancer screening study," **Thorax**, vol. 74, no. 3, pp. 247–253, Mar. 2019.
- [3] R. L. Siegel, K. D. Miller, and A. Jemal, "Cancer statistics," **CA Cancer J. Clin.**, vol. 69, no. 1, pp. 7–34, Jan. 2019.
- [4] M. Oudkerk et al., "European position statement on lung cancer screening," **Lancet Oncol.**, vol. 18, no. 12, pp. e754–e766, Dec. 2017.
- [5] J. Mukherjee, A. Chakrabarti, S. H. Shaikh, and M. Kar, "Automatic Detection and Classification of Solitary Pulmonary Nodules from Lung CT Images," in **Proc. Int. Conf. Emerging Applications of Information Technology (EAIT)**, Kolkata, India, 2014.
- [6] Y. Zhang, B. Dai, M. Dong, H. Chen, and M. Zhou, "A Lung Cancer Detection and Recognition Method Combining Convolutional Neural Network and Morphological Features," in **Proc. IEEE Int. Conf. Computer and Communication Engineering Technology (CCET)**, Beijing, China, 2022.
- [7] M. Liang et al., "Low-Dose CT Screening for Lung Cancer: Computer-aided Detection of Missed Lung Cancers," **Radiology**, vol. 281, no. 1, pp. 279–288, Oct. 2016.
- [8] J. Mai et al., "MHSnet: Multi-head and Spatial Attention Network with False-Positive Reduction for Lung Nodule Detection," in **Proc. IEEE Int. Conf. Bioinformatics and Biomedicine (BIBM)**, Las Vegas, NV, USA, pp. 1108–1114, 2022.
- [9] T. R. Singasani, "Implementing PEGA for enhanced business process management: A case study on workflow automation," *Journal of Scientific and Engineering Research*, vol. 6, no. 7, pp. 292–297, 2019, doi: 10.5281/zenodo.13753108.
- [10] T. R. Singasani, "Comparative analysis of PEGA and MuleSoft: Efficiency, scalability, and user experience," *European Journal of Advanced Engineering and Technology*, vol. 6, no. 3, pp. 152–128, 2019, doi: 10.5281/zenodo.13911215.
- [11] T. R. Singasani, "Integrating PEGA and MuleSoft with cloud services: Challenges and opportunities in modern enterprises," *Journal of Scientific and Engineering Research*, vol. 7, no. 3, pp. 328–333, 2020, doi: 10.5281/zenodo.13884876.
- [12] T. R. Singasani, "Leveraging PEGA and MuleSoft for seamless API integration: A comprehensive framework," *International Journal of Scientific Research*, vol. 9, no. 6, pp. 1955–1957, Jun. 2020, doi: 10.21275/SR210602113108.
- [13] T. R. Singasani, "Leveraging MuleSoft for cloud integration: Exploring API-led connectivity for seamless multi-cloud architectures," *European Journal of Advanced Engineering and Technology*, vol. 7, no. 8, pp. 96–99, 2020, doi: 10.5281/zenodo.13884815.
- [14] O. Ronneberger, P. Fischer, and T. Brox, "U-Net: Convolutional Networks for Biomedical Image Segmentation," in **Proc. Med. Image Comput. Comput.-Assist. Intervent. (MICCAI)**, vol. 9351, pp. 234–241, 2015.
- [15] F. Shi et al., "Semi-Supervised Deep Transfer Learning for Benign-Malignant Diagnosis of Pulmonary Nodules in Chest CT Images," **IEEE Trans. Med. Imaging**, Apr. 2022.
- [16] G. Mu and Y. Chen, "ReLU Cascade of Feature Pyramid Networks for CT Pulmonary Nodule Detection," in **Proc. Int. Conf. Machine Learning in Medical Imaging (MLMI)**, held with MICCAI, Shenzhen, China, 2019.
- [17] A. Agrawal, M. Ansari, and A. Mehrotra, "A Transfer Learning Approach for AI-Based Classification of Brain Tumors," **Mach. Learn. Appl.**, vol. 2, pp. 100003, 2020.
- [18] D. A. Sahu, Y. Nagaraju, K. Sheela Rachel, and V. Venkatesh, "Histopathological Image Classification of Breast Cancer using EfficientNet," in **Proc. Int. Conf. Emerging Technology (INCET)**, Belgaum, India, 2022.
- [19] S. Armato et al., "The Lung Image Database Consortium (LIDC) and Image Database Resource Initiative (IDRI): A completed reference database of lung nodules on CT scans," **Med. Phys.**, vol. 38, no. 2, pp. 915–931, 2011.
- [20] C. Zhao, J. Han, Y. Jia, and F. Gou, "Lung Nodule Detection via 3D U-Net and Contextual Convolutional Neural Network," in **Proc. Int. Conf. Networking and Network Applications (NaNA)**, Xi'an, China, 2018.
- [21] S. Chappidi and A. Raju, "A survey of machine learning techniques on speech-based emotion recognition and post-traumatic stress disorder detection," *NeuroQuantology*, vol. 20, no. 14, pp. 69–79, Oct. 2022, doi: 10.4704/nq.2022.20.14.NQ88010.
- [22] S. Chappidi and A. Raju, "Enhanced speech emotion recognition using the cognitive emotion fusion network for PTSD detection with a novel hybrid approach," *Journal of Electrical Systems*, doi: <https://doi.org/10.52783/jes.644>.
- [23] S. Chappidi and A. Raju, "Advancements in speech-based emotion recognition and PTSD detection through machine and deep learning techniques: A comprehensive survey," *SSRG International Journal of Electronics and Communication Engineering*, vol. 11, no. 5, 2023, doi: 10.14445/23488549/IJECE-V11I5P121.
- [24] S. Chappidi and A. Raju, "Speech-based emotion recognition by using a faster region-based convolutional neural network," *Multimedia Tools and Applications*, Springer, 2024, doi: <https://doi.org/10.1007/s11042-024-19004-2>.